Revealing the conditions of Ni mineralization in the laterite profiles of New Caledonia: Insights from reactive geochemical transport modelling

Andrey Myagkiy, Laurent Truche, Michel Cathelineau, Fabrice Golfier

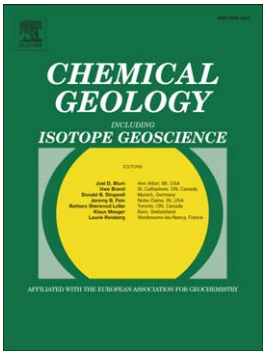

Revealing the conditions of Ni mineralization in the laterite profiles of New Caledonia: insights from reactive geochemical transport modelling

Andrey Myagkiy, Laurent Truche, Michel Cathelineau, Fabrice Golfier

PII: S0009-2541(17)30376-5
DOI: doi:10.1016/j.chemgeo.2017.06.018
Reference: CHEMGE 18375

To appear in: *Chemical Geology*

Received date: 28 September 2016
Revised date: 18 May 2017
Accepted date: 14 June 2017

Please cite this article as: Myagkiy, Andrey, Truche, Laurent, Cathelineau, Michel, Golfier, Fabrice, Revealing the conditions of Ni mineralization in the laterite profiles of New Caledonia: insights from reactive geochemical transport modelling, *Chemical Geology* (2017), doi:10.1016/j.chemgeo.2017.06.018

Revealing the conditions of Ni mineralization in the laterite profiles of New Caledonia: insights from reactive geochemical transport modelling

Andrey Myagkiy[a,*], Laurent Truche[a,b], Michel Cathelineau[a], Fabrice Golfier[a]

[a] *GeoRessources Lab., UMR 7359 of CNRS, CREGU, University of Lorraine, F-54518 Vandoeuvre-Lès-Nancy Cedex, France.*
[b] *ISTerre, UMR 5275 of CNRS, University of Grenoble Alpes, F-38041 Grenoble Cedex 9, France.*

Abstract

New Caledonia is one of the world's largest nickel laterite deposits that form from intense chemical and mechanical weathering of a peridotite bedrock. As a result of such a weathering process a subsequent downward migration of Si, Mg and Ni takes place, which eventually leads to redistribution of the elements in depth and over time depending on their mobility. Being released from ultramafic parent rock to groundwater, the mobility of nickel is to a great extent controlled by sorption, substitution and dissolution/precipitation processes. Therefore, the final profile of nickel enrichment is the result of the superposition of these possible fates of nickel. The way how Ni is redistributed in between them represents and defines its mineralization in laterite. Knowledge of these processes along with factors, controlling them appears to be a key to detailed understanding of laterite formation. In this study a numerical model, which solves the reaction-transport differential equations, is used to simulate the formation of laterite profile from ultramafic bedrock with particular emphasis on modelled Ni enrichment curve, its comparison with in situ observations, and detailed understanding of trace elements mobility. Since nickel deposits in New Caledonia is characterized by oxide and hydrous Mg silicate ores, three different concurrent fates of Ni deposition in a profile were taken into account in the modelling: i) Ni in a goethite crystal lattice, ii) Ni sorbed on weak and strong goethite sorption sites, and iii) Ni precipitated with silicates (garnierite). Simulations were performed using PHREEQC associated with llnl.dat thermodynamic database that has been edited in order to account garnierite minerals used in the calculations. The work outline is represented by: i) long term (10 Ma) simulation of nickel laterite formation and evolution, ii) analysis of mobility of the elements and understanding its controlling factors, iii) comparison of modelled and in situ Ni enrichment profile and analysis of nickel distribution in between different retention processes, iv) modelling and in depth understanding of these retention processes.
The modelling reveals that the vertical progression of the pH front controls thickening of iron-rich zone, explains the vertical mobility of the elements and governs the Ni enrichment. Adsorption itself plays an important role in lateritization process retarding Ni mobility, but i) becomes significant in a narrow range of pH (slightly alkaline) due to competition of Mg and Ni for sorption sites and ii) does not explain such a high nickel content in limonite nowadays, suggesting that Ni is held in goethite mostly by stronger ties i.e. substituted for Fe in the crystal lattice of iron oxyde. 1-D modelling appears to be a powerful tool in understanding the general behavior of trace elements upon the formation of laterite and at the same time reveals that locally Ni mineralizations should be explained by more complex processes, such as lateral transfers, convective flows and preferential pathways.

Keywords: Laterite, Transport Modelling, Weathering, Kinetics, Water-rock interactions

1. Introduction

Nickel laterite ores account for over 60% of global Ni supply (Butt and Cluzel, 2013), thus, making it an important exploration target in anticipation of the future demand of Ni. One of the biggest nickeliferous laterite reserves in the world is located in New Caledonia, 1300 km east of Australia in the south-west Pacific Ocean. Representing around 30% of the

*Corresponding author : ENSG (bat. E), Rue du Doyen Marcel Roubault, TSA 70605, 54518 Vandoeuvre-Lès-Nancy Cedex, France
Email address: andrey.myagkiy@univ-lorraine.fr (Andrey Myagkiy)

global resources in nickel, these laterites are actively worked by various mining companies (SLN-ERAMET, KNS, SMSP etc.).They occur at the top of the obducted ultramafic massif with an average thickness of 30-40 m, resulting from the weathering of the Peridotite Nappe. The initial nickel content of the parent rock, that consists of olivine and various form of serpentine (antigorite, chrysotile, lizardite, polygonal serpentine), can contain up to 0.4 wt% of Ni (Ulrich, 2010; Herzberg et al., 2013; Golightly, 1981). The weathering of the olivine-rich ultramafic rocks and their serpentinized equivalents by meteoric water induces the selective leaching of Fe, Mg, Si and Ni and leads to the formation of a lateritic profile together with an exceptional Ni enrichment (Trescases, 1975; Golightly, 2010). The limonite level, formed at the top of the profile (Fig.1), is mainly composed of iron oxi-hydroxides and followed by the saprolitic level where hydrous Mg silicate deposits form, especially in the mid to lower saprolite. Ni concentration increases constantly throughout the limonite horizon, but the highest Ni grade (locally 2w% up to 5 wt%) is found in the saprolite horizon which represents about one third of the total Ni laterite resources (Fig.1). In this horizon, Ni is concentrated in nickeloan varieties of serpentine, talc-like, chlorite and sepiolite, some of which are poorly defined and known informally as "garnierite" (Butt and Cluzel, 2013). Transition between the saprolite and limonite horizons is marked by a sharp increase in MgO and SiO_2 content and, consequently, by drastic change in mineralogy (Fig.1). The so-called garnierite is mostly located along fractures (Trescases, 1975). Under the saprolite level, a poorly altered peridotite is situated. The basis of the peridotite nappe hosts numerous pure magnesite veins, sometimes associated with amorphous silica (Quesnel et al., 2015).

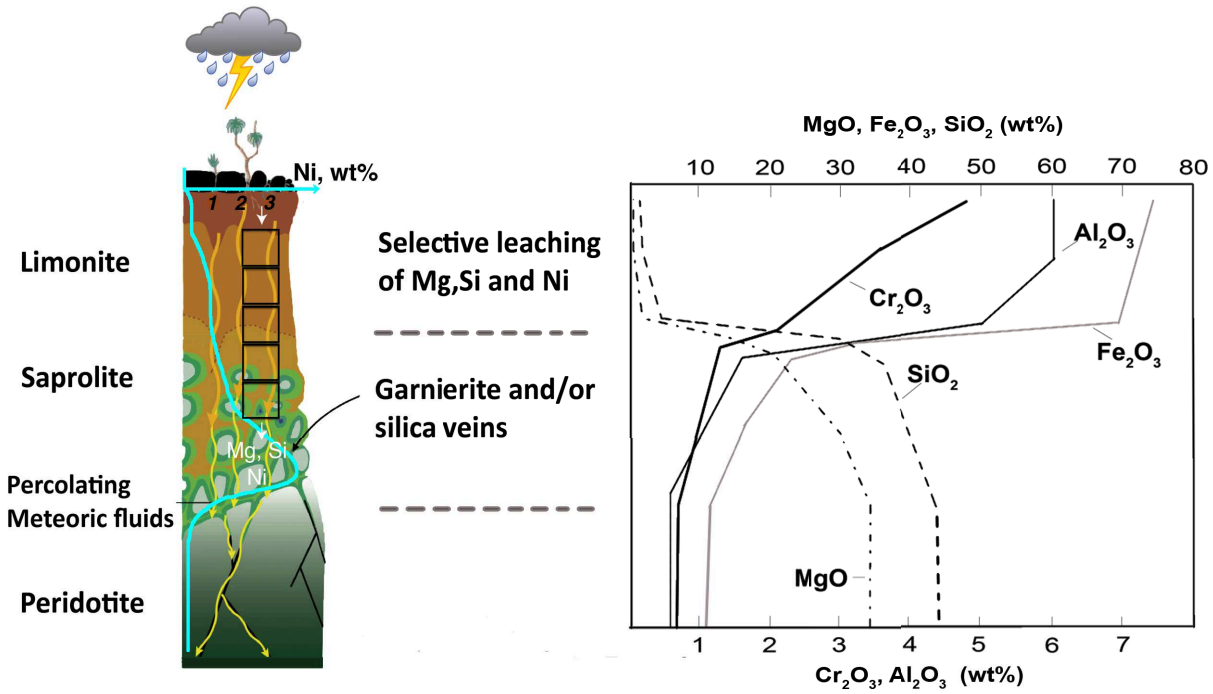

Figure 1: A schematic log of the New Caledonian Peridotite Nappe correlated with approximate elemental composition of different zones. Turquoise line represents nickel distribution in a profile. Modified after (Ulrich et al., 2011; Troly et al., 1979; Guilbert and Park, 1986)

The enrichment of nickel in the weathering profile is governed by many interplaying factors that include mineralogical composition of parent rock, climate, chemistry and rates of chemical weathering, tectonics, and drainage (Lelong et al., 1976; Golightly, 1981, 2010; Gleeson et al., 2003; Freyssinet et al., 2005; Butt and Cluzel, 2013). After being leached from rock-forming minerals nickel is thought to be redeposited be-

low, mostly associated with i) Ni-rich ferruginous oxide ore where it is sorbed and/or substituted for Fe in the crystal lattice (Cornell, 1991; Fischer et al., 2007; Singh et al., 2002; Carvalho-e-Silva et al., 2003; Dublet et al., 2012), ii) a wide variety of neo-formed silicate minerals such as talc-like and sepiolite-like minerals (Cathelineau et al., 2015; Villanova-de-Benavent et al., 2014; Wells et al., 2009), and iii) partly weathered primary lizardite, in which Mg to different extent has been exchanged by Ni (Golightly, 1981, 2010). Three different mechanisms have been suggested in the literature in order to explain the association between nickel and goethite: i) isomorphous substitution of Ni for Fe into the goethite structure, ii) association of Ni with poorly crystalline phase, and iii) adsorption of Ni to goethite surface. Singh et al. (2002) and Carvalho-e-Silva et al. (2003) found and confirmed using EXAFS that Ni^{2+} is associated with goethite via isomorphous substitution for Fe^{3+}. Using sequential leaching studies of Indian laterite samples Swamy et al. (2003) reported that the quantity of chemisorbed Ni was negligible and most of the nickel was bound in the crystal lattice with some associated with amorphous goethite. Actually such an association is quite complex and literature suggests that there is a continuum going from one stage to other (Davis et al., 1987; Stipp et al., 1992). Therefore, an initial fast adsorption step is followed by a slow step of incorporation of the adsorbed species into the crystal structure with formation of solid solution. Schultz et al. (1987) experimentally documented the irreversible adsorption of metals on ferrihydrite surfaces. Adsorption/desorption of 10^{-5} M Ni^{2+} on 10^{-3} M ferrihydrite revealed that after the overnight exposure only about 25 % of the Ni^{2+} could be desorbed and the remainder stayed bound in the ferrihydrite structure. Similar hysteresis were found by McKenzie (1980), Brümmer et al. (1988), Barrow et al. (1989), and Gerth et al. (1993). Further recrystallization of the ferrihydrite leads to a release of the nickel over time. Direct evidence was established for a negative correlation between the bulk Ni content and the crystallinity of goethite as a function of depth in the New Caledonian Ni laterites (Dublet et al., 2012, 2015).

There are a number of scientific articles dealing with modelling of regolith formation from bedrock. For example Soler and Lasaga (1996, 1998) have been working on an advection-dispersion-reaction model of bauxite formation, Fletcher et al. (2006) and Lebedeva et al. (2007) on granite bedrock (albite + FeO-bearing phase + quartz) transformation to saprolite (goethite + kaolinite + quartz), Navarre-Sitchler et al. (2011) on a reactive transport model for weathering rind formation on basalt etc. Nevertheless, the mobility and transport of trace elements in ultramafic bedrock was not yet modelled with the only exception of a recent study by Domènech et al. (2017). Their work provides valuable insights into the formation of the different laterite horizons in the profile from partially serpentinized peridotite. However, the analysis seems to miss important elements that suggest Ni should be included into the goethite structure and cannot be explained by adsorption alone. In addition, the formation of garnierite is not considered and Ni enrichment is shown only in oxide part of deposits. Thus, the processes of Ni retention in a profile and their controlling parameters are still poorly understood.

In the present work, we used a reactive transport modelling in order to study the development of the secondary nickel ores upon vertical progression of the alteration front. We analyse the effect of key parameters governing i) sorption processes on a goethite surface , ii) precipitation/dissolution of secondary minerals, and iii) kinetic dissolution of serpentinized olivine due to meteoric water flow (Fig.2). Moreover, the effect of pimelite/kerolite (Ni-bearing phases) being present as a solid solution and incorporation of Ni into the goethite structure were also studied. The role of sorption processes on goethite in Ni redistribution in space during the mineralization, as well as the detailed understanding of their mechanisms have particular emphasis in this paper. Direct comparison of Ni distribution obtained after the modelling with its typical distribution in the profiles provides us in depth understanding of the weathering process in laterite deposits, reveals the validity of the model and gives new insights into the other processes that might have also governed the mobility of elements and formation of these increasingly important Ni deposits.

2. Materials and methods

2.1. Modelling the hydrodynamic system

A reactive multicomponent 1-D transport model of supergene enrichment of lateritic Ni deposits has been simulated by assuming the weathering of a one-dimensional vertically oriented column of serpentinized olivine due to steady state meteoric water flow. The code used for the simulations is PHREEQC (V 3.1.4) (Parkhurst and Appelo, 2013). The 1-D column is defined by a series of 40 cells of 0.5 m. in length. The velocity of water in each cell is determined by the length of the cell, porosity and amount of annual rain precipitation. Solute concentrations at some point on a flow-line may change by i) advection of concentration gradi-

ents, ii) reactions with the solid material, and iii) dispersion and diffusion. The Advection-Reaction-Dispersion equation that describes these changes along the flowline and implemented on Phreeqc is the following:

$$\left(\frac{\partial c}{\partial t}\right)_x = -v\left(\frac{\partial c}{\partial t}\right)_t - \left(\frac{\partial q}{\partial t}\right)_x + D_L\left(\frac{\partial^2 c}{\partial x^2}\right)_t \qquad (1)$$

where c is the solute concentration ($mol.l^{-1}$), v is pore water flow velocity ($m.s^{-1}$), D_L is hydrodynamic dispersion coefficient ($m^2.s^{-1}$) and q is the concentration in the solid ($mol.l^{-1}$ of pore water). In our calculations we neglect dispersion and set D_L to 0. According to in situ observations, indeed, transport of the chemical components is controlled by advection and high reaction rates. Neglecting dispersion will cause sharper reaction front and higher concentration peaks. In other words, spreading of the concentration front should be slightly underestimated.

Flux boundary conditions (Cauchy) were defined for the first and last cell. A slightly acidic tropical rainwater with pH=5.6 due to its equilibrium with atmospheric CO_2 represents an incoming solution and is injected in the first cell (Fig.3). Regarding separately the values of the experimental rates of kinetic dissolution of the parent rock constituents (olivine, serpentine, enstatite), presented in the literature (*e.g.* Brantley and Chen (1995); Pokrovsky and Schott (2000); Wilson (2004); Thom et al. (2013)), one may note that olivine has a highest rate of the dissolution process among them. The rates of enstatite and serpentine are extremely sluggish compared to those of olivine, being one to a few orders of magnitude lower depending on pH. This makes olivine the main initial mineral in a system that provides nickel and other elements (Mg, Si and Fe). In this way, the numerical modelling was performed assuming olivine in each cell of the 1-D column at initial state (Fig.2).

Porosity of the ultramafic bedrock was chosen to be about 2% but is highly dependent on the fractures density (Join et al., 2005; Jeanpert and Dewandel, 2013). Due to code limitations, the porosity remains constant throughout the calculations. There are some other codes with improved hydrodynamic part (PhreeqcRM, Crunchflow, etc) that handle porosity changes but from a 1-D modeling point of view such an assumption has a minor influence on the results of simulation. Indeed, when magnesium and silica are leached from limonite zone a total mass loss of up to 70-80% appears there. At the same time, the density ahead of the pH front, where silicates form, will still be much closer to the initial value than in the goethite zone. Since 1-D column does not allow any kind of lateral fluid movements, the fluid flow rate is constant along the column. In real profiles, the goethite zone density is so low that it collapses under the weight of the profile to a near constant value (Golightly, 1981).

The New Caledonia is situated in seasonally humid wet savannas, thus, characterized by summer rainfall of 900-1800 mm and a 2-5 months winter dry season (Butt and Cluzel, 2013). Nevertheless, these values are related to the current climatic circumstances and most likely were not the same during all 10 Ma of laterite formation. According to calculations of Thorne et al. (2012) Ni laterites develop where rainfall exceeds 1000 mm/y and mean monthly temperatures range between 22-31°C (summer) and 15-27°C (winter). For our simulations the value of 2000 mm/y was chosen as acceptable.

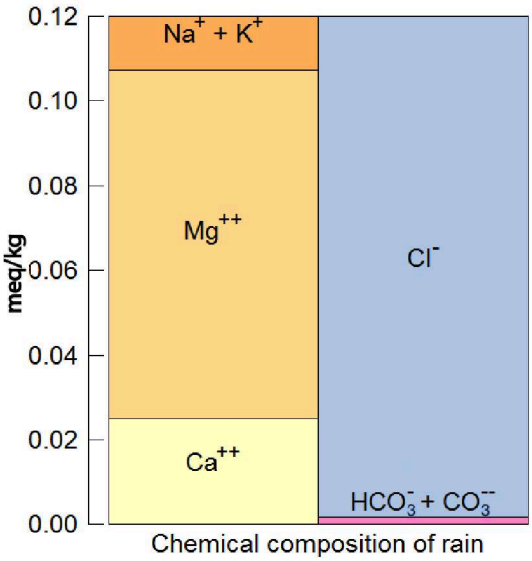

Figure 3: Bar chart of chemical composition of incoming solution (rainwater) at equilibrium with atmospheric CO_2 and subsequent pH of 5.6. In accordance with Trescases (1975).

The total computing time for 1-D transport calculations is defined as 250,000 pore volumes of filling solution that are moved through the column (10^7 shifts of

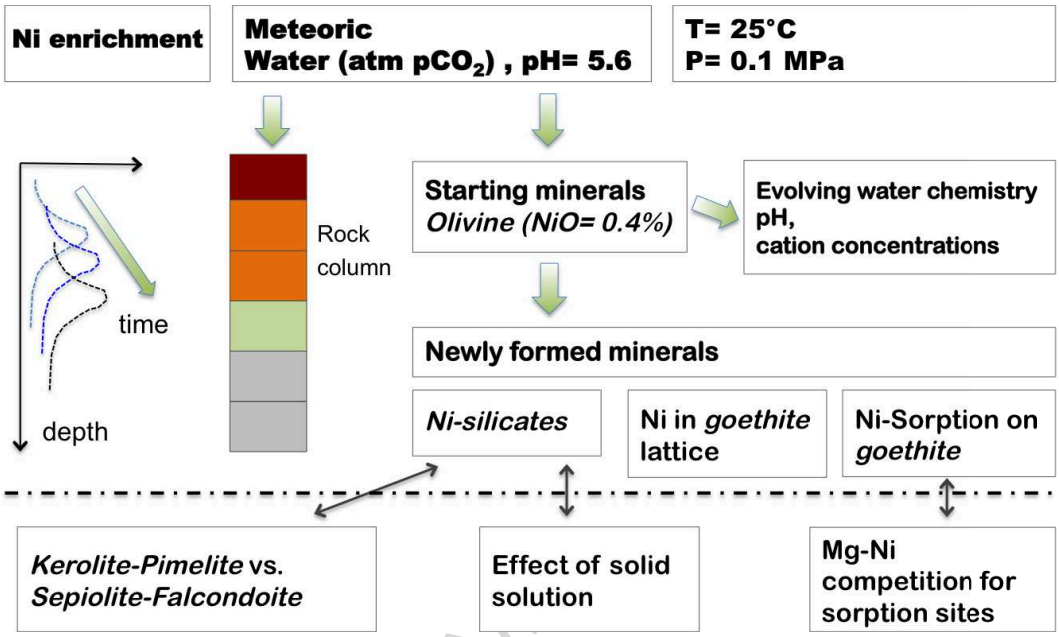

Figure 2: Interaction between a rock column and meteoric water: main variables taken into account.

solution per 40 column cells). The real geological time in years could be estimated from residence time of solution in a cell multiplied by number of solution shifts. Since the residence time per cell was defined as 100,000 seconds, it will correspond to a summary computing time of about 10 Ma. We take this value as a connection of our results to real geological time but it should be noted that in reality the residence time will greatly change (decrease) due to porosity changes, formation of fractures and lateral dissipations of fluid. Therefore, this value of 10 Ma is an upper limit and certainly overestimated. Further planned investigations will require implementation of this code into a 2D/3D fully coupled hydrological model to resolve this drawback.

2.2. Modelling the geochemical system

Olivine composition in the model was selected according to Trescases (1975) as following: $Mg_{1.82}Fe_{0.17}Ni_{0.01}Al_{0.006}SiO_4$. Olivine dissolution is assumed to be kinetically controlled whereas the precipitation of secondary weathering products is considered to occur according to local equilibrium. Pokrovsky and Schott (2000) provided in their work the following steady state specific dissolution rate for olivine at 25°C in CO_2-free solutions:

$$log(r) = -0.5pH - 6.64 \quad (2)$$

Which is consistent with an Arrhenius equation of the form of:

$$r = Aa^n_{H^+} exp(-E_a/RT) \quad (3)$$

where r signifies the specific dissolution rate of olivine in $(mol.m^{-2}.s^{-1})$, a^n_H+ is the activity of protons $(mol.l^{-1})$, A refers to a pre-exponential factor, E_a designates an activation energy, R represents the gas constant, and T denotes absolute temperature.

Generally, the effect of atmospheric CO_2 on olivine dissolution rate is very weak in acid to neutral solutions but may be important in alkaline conditions. Results of Wogelius and Walther (1991) show a decrease of the dissolution rate at elevated pH and low CO_2 pressure while experiments conducted under similar conditions by Pokrovsky and Schott (2000) and Golubev et al. (2005) did not account such a decrease in comparison with their CO_2-free experiments. Current modelling was performed according to the equation (2) and without taking into account the effect of presence of CO_2.

The overall olivine reaction rate in the model is as follows:

$$R_d = r\left(\frac{A_0}{V}\right)\left(\frac{m}{m_0}\right)^n \quad (4)$$

where R_d signifies the overall reaction rate $(mol.l^{-1}.s^{-1})$, r is the specific dissolution rate $(mol.m^{-2}.s^{-1})$ extracted from equation (2), A_0 refers to

the initial surface area of the solid (m^2), V designates the volume of solution (l), m_0 represents the initial moles of solid, and m is the moles of solid at given time.

The factor $(m/m_0)^n$ accounts for changes in surface area during dissolution of olivine. For a monodisperse population of uniformly dissolving spheres or cubes, n = 2/3, since m is proportional to the volume, or r^3 (here r is the radius of the sphere or the side of the cube), while the surface area is proportional to r^2.

The rate expression is embedded in the PHREEQC third order Runge-Kutta-Fehlberg algorithm (Parkhurst and Appelo, 2013). Equilibrium phase composition is calculated before a kinetic calculation is initiated and after a kinetic reaction increment. Calculations were done at 25°C with the code PHREEQC associated with the llnl.dat thermodynamic database (Johnson et al., 2000), that has been edited in order to account for garnierite minerals. The reactions, involved in the precipitation or dissolution of Mg and Ni end-member phyllosilicates are given in Table 1.

Basically, Mg-Ni-phyllosilicates are parts of solid-solution series extending from Mg to Ni end-members (*e.g.* Springer (1974, 1976); Reddy et al. (2009)) and effect of them being present as an ideal solid solutions instead of separate minerals will be discussed. The process of substitution of Ni for Mg in the lattice of serpentine is not considered here due to the lack of thermodynamic data needed to perform such kind of modeling. Trescases (1975) demonstrated that many ground waters from the base of the nickel laterite profiles in New Caledonia are saturated or supersaturated with respect to talc-like mineral but rarely saturated in serpentine. For the moment serpentine has been seldom reported to form under earth-surface conditions and, thus, suppressed from equilibrium phases that were allowed for precipitation. Instead, in nature the precipitation rates favor the formation of metastable sepiolite and kerolite in Al-poor environments (Stoessell, 1988). Thus, for transport calculations at 25°C the list of secondary weathering products is following: Ferrihydrite, Gibbsite, Saponite-Mg, Kerolite, Pimelite, Sepiolite, Falcondoite, Quartz. Ferrihydrite is known to be an initial precursor phase in the formation of goethite but is difficult to be identified using standard characterisation techniques (such as PXRD) due to its poorly crystalline nature. According to Cornell et al. (1992) the introduction of nickel to the system increases the stability of the ferrihydrite phase, inhibiting its transformation to goethite and also suggesting that ferrihydrite could be still present in nickeliferous laterites. Goethite and hematite form later on from ferrihydrite and the ratio and cristallinity of these products are strongly influenced by pH. Schwertmann and Murad (1983) showed that at 24°C maximum hematite was formed in between pH 7 and 8, while maximum goethite at pH below 4 and above 12. This way, relying on a diagram of pH change with depth, one can suppose what will be the final products in each part of profile.

The surface complexation model of Dzombak and Morel (1990), that takes into account binding of metals and protons on both strong and weak sites of ferrihydrite, which develops a charge depending on the ions sorbed, has been used in order to simulate adsorption process. The adsorption constants required to parameterize the model for Ni adsorption at the surface of ferrihydrite were obtained by fitting experimental data (Dzombak and Morel, 1990) and are given in Table 2.

Two sites are defined for a diffuse-double-layer: i) Hfo_s, which is strong binding site, and ii) Hfo_w, which is weak binding site. Dzombak and Morel (1990) used 0.2 mol weak sites/mol ferrihydrite and 0.005 mol (2.5% of weak sites) strong sites/mol ferrihydrite with a surface area 5.33×10^4 ($m^2.mol^{-1}$) and a weight of 89 g Hfo/mol Fe. To be consistent with their model, the relative number of strong and weak sites is kept constant as the total number of sites varies. In reactive 1-D transport modeling presented in this paper oxi-hydroxide surfaces change in proportion as the ferrihydrite dissolves or precipitates.

Table 2: Thermodynamic data for a diffuse-double-layer surface "Hfo"(Hfo stands for hydrous ferric oxide, i.e. ferrihydrite), derived from Dzombak and Morel (1990).

Reaction	**Log k**
$Hfo\_sOH + H^+ = Hfo\_sOH_2^+$	*7.18*
$Hfo\_sOH = Hfo\_sOH^- + H^+$	*-8.82*
$Hfo\_sOH + Ni^{2+} = Hfo\_sONi^+ + H^+$	*0.37*
$Hfo\_wOH + H^+ = Hfo\_wOH_2^+$	*7.18*
$Hfo\_wOH = Hfo\_wOH^- + H^+$	*-8.82*
$Hfo\_wOH + Ni^{2+} = Hfo\_wONi^+ + H^+$	*-2.5*

It is worth noting that the llnl.dat database contains thermodynamic data for sorption of many trace metals. Once surface Ni complexes, Hfo_s and Hfo_w, are introduced in the model, the effect of other cations, such as Mg^{2+}, Fe^{2+}, Ca^{2+} can be accounted for. Cations

Table 1: Dissolution reactions for Mg and Ni end-members of garnierite and Saponite-Mg, with the corresponding equilibrium constants at 25°C and 1 bar.

Mineral	Reaction	Log K
Kerolite	$Mg_3Si_4O_{10}(OH)_2 : H_2O + 6H^+ = 3Mg^{2+}+4SiO_2+5H_2O$	*25.79 (Stoessell, 1988)*
Pimelite	$Ni_3Si_4O_{10}(OH)_2 : H_2O + 6H^+ = 3Ni^{2+}+4SiO_2+5H_2O$	*11.46 (Nriagu, 1975)*
Sepiolite	$Mg_4Si_6O_{15}(OH)_2 : 6H_2O + 8H^+ = 4Mg^{2+}+6SiO_2+11H_2O$	*30.44 (Stoessell, 1988)*
Falcondoite	$Ni_4Si_6O_{15}(OH)_2 : 6H_2O + 8H^+ = 4Ni^{2+}+6SiO_2+11H_2O$	*12.31 (Nriagu, 1975)*
Saponite-Mg	$Mg_{3.16}Al_{0.33}Si_{3.67}O_{10}(OH)_2 + 7.32H^+ = 3.16Mg^{2+}+0.33Al^{3+}+3.67SiO_2+4.66H_2O$	*26.25 (llnl.dat)*

competition for sorption at the surface of ferrihydrite will, thus, influence the mobility of leaching metals. In order to analyse this competition a transport modelling through one-cell with flux-open boundaries was performed. The input of one-cell model is identical to the main one with 40 cells. This model has been used in order to reduce calculation time and gain insight into the aforementioned competition of metals for sorption sites and precipitation of Ni-goethite solid solution with 2wt% of Ni. It should be noted that in a results and discussion section we always use the name goethite in spite of the fact simulations are done with ferrihydrite constants (same chemical formula and different solubility constant value). This latter choice is applied to avoid any kind of confusions since ferrihydrite is being more geochemical rather than geological term.

3. Results and discussion

3.1. 1-D Reactive transport model

Figure 4 shows the evolution of the paragenetic sequence and the development of the secondary nickel ores as a function of time. The results represent mass fractions of secondary weathering products formed after 50,000 PV, 150,000 PV and 250,000 pore volumes (PV) of filling solution that are moved through the column and corresponds to 2 Ma, 6 Ma and 10 Ma, respectively. The reactive transport model reproduces both the formation of the laterite profile in time with thickening of iron-rich zone and change of the Ni content with depth. Here, nickel supplied in the system by olivine dissolution was supposed to be redistributed in between solution, adsorption on goethite and dissolution/precipitation of Ni-bearing minerals. In the following chapter of detailed understanding of Ni behaviour during weathering is displayed. As can be seen from Figure 4, the obtained chemical profile clearly distinguishes the ferruginous/aluminous residual part where Si, Mg, and Ni are leached, from the zone where silicates start to precipitate. The effect of silicate weathering on the water chemistry is primarily the addition of cations (Ni^{2+}, Mg^{2+}, Fe^{2+}, Fe^{3+}; Al^{3+}) and silica. pH variation is balanced on one hand by silicate weathering reactions which consume H^+ and on the other hand by leaching of the elements out of the cell and renewing with low pH meteoric water which tend to decrease the pH value. Migration of the pH front, subdividing slightly acidic at the surface to alkaline pH at depth, appears to have the main influence in controlling the precipitation/dissolution of neo-formed silicate minerals, and, thereby, regulating the transport of elements in the profile. The limonite zone is represented by goethite and minor precipitations of gibbsite. Beneath, after the pH front, the secondary weathering products are represented by falcondoite (Ni bearing phase), and massive precipitations of sepiolite and Saponite-Mg. Considering the results after 2 Ma, one can observe that part of olivine mass is not yet dissolved, providing pH up to 11 at the bottom of the column, and that pimelite (Ni talc-like) precipitation (indicated by a narrow black line on Fig.4) occurs at depth, after the pH front. Pimelite precipitation is no more observed after 4 Ma. Indeed, after 4 Ma, olivine disappears and the maximum pH value decreases from 11 to 9.5 after the pH front.

It worth noting that in New Caledonia the silicates, precipitated in fractures or in a form of concentric zoning of Ni-bearing silicates (Cathelineau et al., 2016), are mostly represented by talc-like minerals. This is in contrast to sepiolite-like phases (falcondoite, sepiolite), obtained in current numerical modelling which is more common for Falcondo Ni-laterite deposits observed in Dominican Republic (Villanova-de-Benavent

et al., 2014). In order to find out why sepiolite-like precipitated instead of talc-like minerals let us turn to the literature. According to Stoessell (1988) the difference in solubility between kerolite and sepiolite is small enough that precipitation kinetics is probably decisive in their formation. The metastability of kerolite relative to sepiolite, determined in the study of Stoessell (1988), was suggested by Jones (1986). He reported kerolite as a precipitate at Stewart springs (California, USA) from waters with pH above 12, but with aqueous silica concentrations below (25°C and 1 bar) quartz saturation. Jones (1986) suggested that with increasing pH and Mg content in water and decreasing silica content, kerolite should precipitate at the expense of sepiolite. Same conclusion might be reached for pimelite (Ni talc-like) and falcondoite (Ni sepiolite) precipitation since they are the Ni counterparts of kerolite and sepiolite, respectively.

It is consistent with the numerical results (Fig.4) where, as it was mentioned above, pimelite (narrow black line, 2 Ma column) precipitated in the deeper part of profile where high pH of about 11 was maintained by dissolution of still presenting olivine. In this way it could be concluded that for precipitation of talc-like minerals at 25°C in Al-poor environments it is necessary and sufficient to have an ample amount of olivine in a system.

It should be noted that in real profiles olivine would persist for longer time due to the different character of the porosity distribution. In fact, the extreme instability of olivine results in its replacement by silicate phases in situ with the cations in the solutions diffusing outwards to joints, where the water is flowing downwards. Because of this the olivine in the bulk material does not disappear before 6 million years as in the model. Nevertheless, an accurate representation of the process will not be achieved until 2D modelling is attempted.

Returning to the results of the model the entire dissolution of olivine in the column after 6 Ma and 10 Ma (Fig.4) led to a change in pore water pH with values of 5.6 close to the surface to about 9.5 at the bottom. Present day water analyses at Koniambo (northwest of New Caledonia) indicated similar pH condition: from 5.5 near the surface to about 10 at depth, either in the laterite or in the serpentinized peridotite (Jeanpert and Dewandel, 2013). Concerning the mass fraction of Ni bearing sepiolite (falcondoite), its accumulation and downward movement with pH front migration can be observed. The increase of Ni content with time and depth is shown in Figure 5.

It should be noted that the Ni concentration in wt% here is related to initial mass of olivine in a cell, serving as reference in order to be able comparing it through time. Normalizing to the current mass of minerals presented in a cell adds a complexity in following comparison of Ni enrichment since this mass is changing due to the leaching. Despite the fact that in the Figure 5 at 250,000 PV (10 Ma) maximum concentration of nickel (4.8 wt.%) seems to be lower than in previous step (6 wt.% after 200,000 PV, or 8 Ma), it appears that the thickness of the Ni rich zone is also higher after 250,000 PV than after lower PV circulation. Therefore, the precipitation of Ni in the two closest cells after 250,000 PV (10 Ma) (Fig. 4) with Ni content of 3.06 wt.% and 4.80 wt.% at 9.25 m and 9.75 m of depth respectively, yields an overall equivalent Ni content of 7.89 wt.%. This value is much higher comparing to typical New Caledonian profile presented in Figure 1 which exhibits up to 2-3 wt.% of Ni distributed throughout limonite and saprolite zone. The cause of it might be related to precipitation of silicates at local equilibrium in our model, implying that simultaneous precipitation occurs once favorable conditions are reached in a cell and resulting in a narrow zone of Ni precipitation. Also, in nature, nickel, released due to peridotite dissolution, may be partly lost by lateral movement in solution.

The overall concentration of nickel of 7.89 wt.% at the last step of simulation (10 Ma) represents 97.2 % of the initial nickel content in the column and distributed as follow: i) 4.27 wt.% of Ni sorbed on ferrihydrite surface, ii) 95.7 wt.% precipitated with Ni-silicate (falcondoite) and iii) 1.69×10^{-4} % in solution along the whole column. From Figure 5 one can observe the movement of transition zone from the limonite horizon to the saprolite, which is marked by a sharp increase in MgO content from 0 to up to 20 wt.%. Iron content meanwhile varies from values of about 65 wt.% before the reaction front down to 5 wt.% after it. Whilst the iron has been oxidized, the nickel remains bivalent and is somewhat mobile, more so than iron, less so than magnesium. This chemical distribution of elements is consistent with Figure 1 and clearly distinguishes the ferruginous residual part where Si, Mg, and Ni are leached and Mg discontinuity zone appears.

Nevertheless, in Figure 1 Ni concentration is increasing throughout limonite zone up to 2 wt.% at the con-

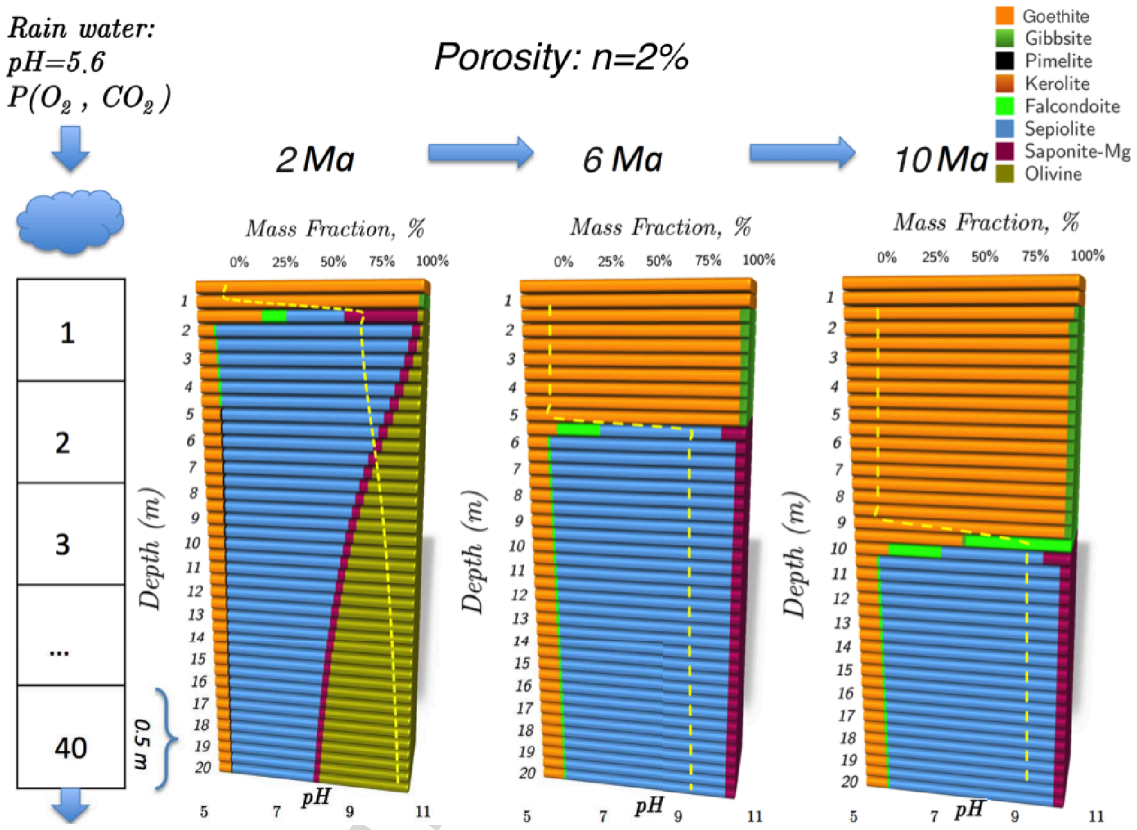

Figure 4: Mass fraction of secondary weathering products after 50,000 PV (2 Ma), 150,000 PV (6 Ma) and 250,000 PV (10 Ma). Yellow dotted line represents current pH front in the column.

tact with saprolite, while in numerical modelling this zone comes out to be free of Ni. According to the modelling results, adsorbed nickel appears to be governed by pH front. Being initially retarded compared to fluid movement, adsorbed Ni has been eventually liberated into pore water at pH as low as 5.6 due to reaction front downward advancement upon silicates dissolution. Dependence of nickel sorption on pH along with competitive retardation is discussed in the following chapter, devoted to a detailed understanding of the weathering process. Yet, it could be concluded that adsorption can not explain such a high nickel content in limonite nowadays since the actual pH of soil waters can be in some instances as low as 4.5 due to dissolved organic acids, thus, suggesting that nickel is held here by stronger ties. The latter might be explained by isomorphous substitution of Ni for Fe in goethite and either significant process in soils related to specific binding of elements to the variable charge surfaces of organic matter. Adsorption on organic matter is similar to that on ferrihydrite since surface charge likewise depends on pH and solution composition, but the difference is that the sorption edge for organic matter is shifted to lower pH. It implies that at low pH from about 4 to 7 adsorption on organic matter will be dominating, but at higher pH the major role will be passed to adsorption on oxyhydroxides. Present study does not consider the issue of DOC due to its low concentration in well-drained and scarce in terms of soil terrains of New Caledonia.

3.2. Detailed understanding of the weathering process

3.2.1. Effect of pimelite/kerolite being present as solid solution

The numerical simulations presented above consider the Mg-Ni-phyllosilicates to be pure end-members although in reality they are being members of solid-solution series extending from Mg and Ni end-members (*e.g.* Springer (1974, 1976); Reddy et al. (2009); Villanova-de-Benavent et al. (2014); Cathelineau et al. (2015)). Usually solid solutions show deviations from ideal behavior and the activity coefficients, that account for non-ideality, become a function of the excess free energy of mixing. The free energy of mixing might be

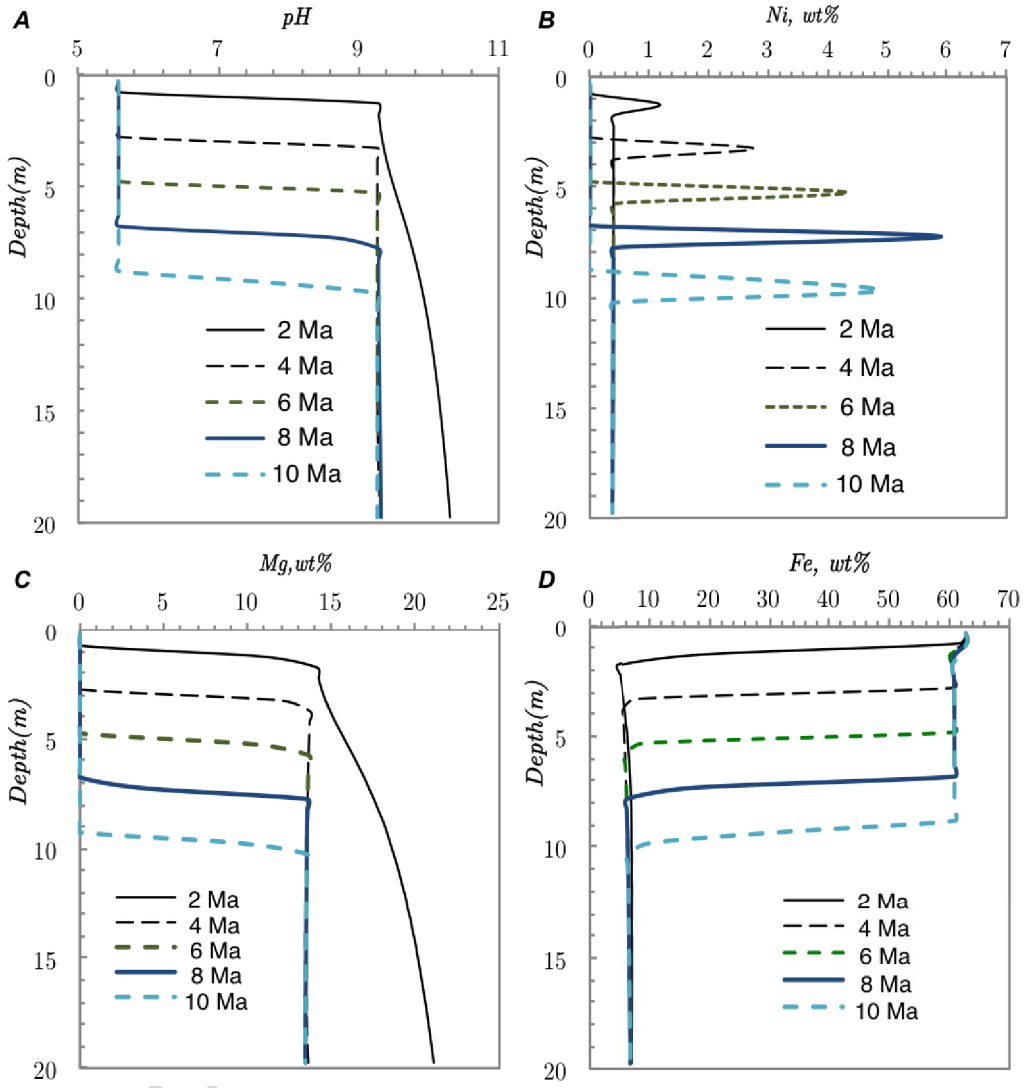

Figure 5: Migration of pH front along the profile with corresponding Ni, Mg and Fe concentrations in the secondary weathering products.

obtained from different non-ideal thermodynamic properties such as variations in fractionation factor, miscibility gaps etc. (Glynn, 2000). Despite the fact that many researchers describe Mg-Ni-phyllosilicate members of solid solutions, the possibilities of modelling such a system remain poor due to the lack of thermodynamic data, thus, limiting simulations by assumption of ideality. In this way, for example, Galí et al. (2012) have calculated Lippmann diagrams for the garnierite solid solutions. This subchapter aims at understanding the effect of e.g. pimelite and kerolite being present as a solid solution instead of separate mineral phases. Linear combination of reactions for kerolite and pimelite, presented in Table 1 results in Equation (5):

$$Mg_3Si_4O_{10}(OH)_2 : H_2O + 3Ni^{2+} = Ni_3Si_4O_{10}(OH)_2 : H_2O + 3Mg^{2+} \quad (5)$$

At first, let us consider a situation where a solution is in equilibrium with kerolite and pimelite as separate minerals. The mass action expression for Equation (5) looks as follows:

$$K = \frac{[Ni_3Si_4O_{10}(OH)_2 : H_2O]}{[Mg_3Si_4O_{10}(OH)_2 : H_2O]} \times \frac{\left[Mg^{2+}\right]^3}{[Ni^{2+}]^3} = \frac{K_{Kerolite}}{K_{Pimelite}} = 10^{14.33} \quad (6)$$

Then, in Equation (6) the activities of two pure solid phases will be equal to one. Therefore, the ratio $\frac{[Mg^{2+}]^3}{[Ni^{2+}]^3}$ in solution is fixed to $10^{14.33}$ and $\frac{[Mg^{2+}]}{[Ni^{2+}]} = 59795$. The concentration of $\left[Ni^{2+}\right]$ is much smaller than of $\left[Mg^{2+}\right]$ because the solubility of pimelite is much smaller than of kerolite.

In the second situation $\left[Ni^{2+}\right]$ is incorporated in the kerolite structure as an ideal solid solution, which may be written as $Ni_\lambda Mg_{3-\lambda}Si_4O_{10}(OH)_2 : H_2O$, where λ represents the nickel mole fraction. In this way, activities of kerolite and pimelite in Equation (6) will no longer be equal to one as for separate minerals, but will depend on λ . Therefore, if Mg concentration remains the same as before, then the Ni concentration must now be lower. It can clearly be seen in Figure 6, that shows the effect of Ni substitution in pimelite/kerolite solid solution on the relative Ni concentration decrease in solution. Therefore, the common values of Ni mole fraction in New Caledonian pimelite/kerolite solid solutions, *i.e* around λ = 0.3-0.4, will lead to a decrease of the Ni concentration by about 20% from the case with pure phases on assumption that Mg concentration remains the same (Fig.6).

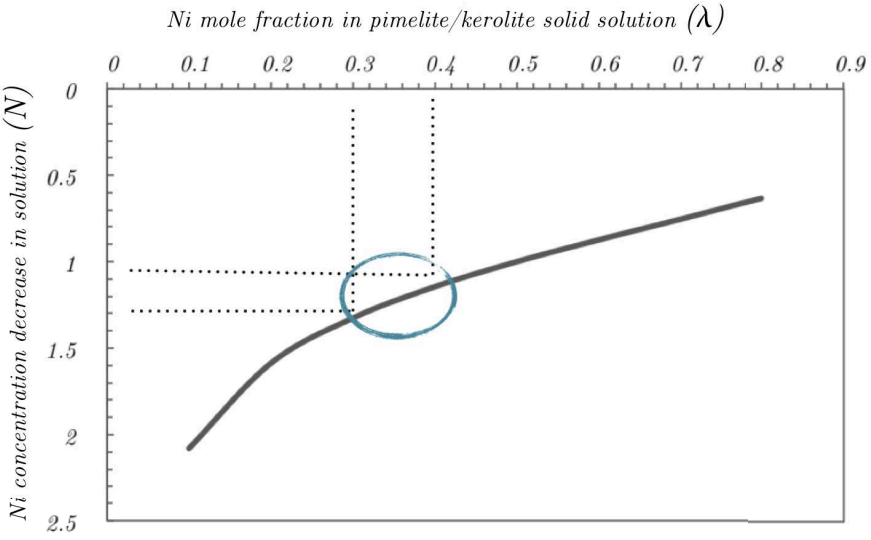

Figure 6: Effect of Ni substitution in pimelite/kerolite solid solution (λ) on the relative Ni concentration decrease in solution (N).

Thus, to conclude it should be said that the formation of solid solution lowers the aqueous concentration of the minor component, in our case nickel, but does not have a drastic effect on the global Ni mass balance. The latter means that despite the use of separate mineral phases our results of simulations may be considered as reliable.

3.2.2. Ni in solid solution with goethite

It has already been mentioned above that sorption alone cannot explain increase of Ni content throughout the limonite zone (Fig.1). In our 1-D model all Ni, adsorbed on goethite, was released in solution and shifted at depth once the pH decrease below six after the front. Obviously, this latter phenomenon is not observed in the field, where Ni still persists in the limonite zone. According to Dublet et al. (2012), nickel content up to 2wt.% is common for New Caledonian laterites, where

Ni^{2+} is associated with goethite via isomorphous substitution for Fe^{3+}. In order to account for this gap, here, we perform a sensitivity test that considers additionally to our previous transport model (Fig.4) a precipitation of Ni-bearing goethite. In this way, reaction for precipitation of Ni-bearing goethite has been added in the thermodynamic database as follows:

$$Fe_{0.98}Ni_{0.03}OOH + 3H^{+} = 0.98Fe^{3+} + 0.03Ni^{2+} + 2H_2O \quad (7)$$

The influence of such a small amount of Ni in structure of goethite on its equilibrium constant has been neglected. Indeed, this constant, according to Equation (7), will be defined as:

$$LogK = 0.98 \times log\left[Fe^{3+}\right] + 0.03 \times log\left[Ni^{2+}\right] + 3pH \quad (8)$$

Considering that the Ni concentrations in the model are as low as 10^{-9} to 10^{-6} moles per liter, and taking into account Equation (8) one can see that the effect of Ni presence on the equilibrium constant will be minor.

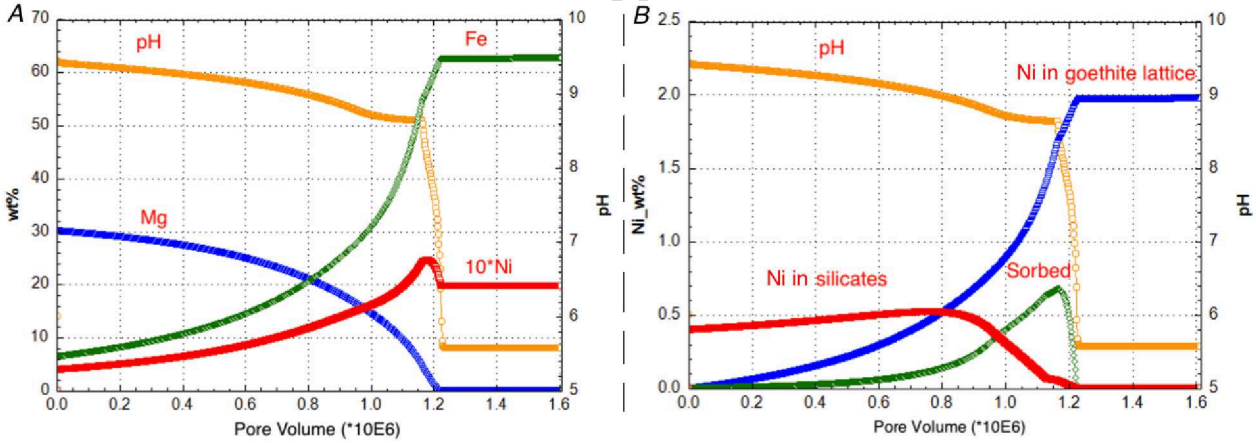

Figure 7: ***A*** represents the mobility of the elements in a 1-D reactive transport modelling through one cell; supergene enrichment of Ni and its retention by three different mechanisms: i) Sorption on goethite surface, ii) Retention in goethite structure, and iii) Precipitation with Ni-silicates. ***B*** shows the split (redistribution) of Ni between different retention mechanisms upon the formation of laterite.

Figure 7(*A*) shows the chemical distribution of the elements in minerals versus pore volume (one million of PV represents one million years). Current reactive transport modelling has been performed through one cell with flux-open boundaries instead of 40 cells column. Incoming solution, olivine content and dissolution rate here are identical to those used in 1-D transport model previously presented and such a test case was done in order to get detailed understanding of the weathering processes in each cell. X-axis in Figure 7 represents pore volumes, which is a number that shows how many times filling solution moved through the cell. Therefore, this axis represents time of evolution of the bedrock until the formation of oxide-rich zone. This way the principal shape Ni enrichment curve in Figure 7(*A*) can be easily compared to Figure 1. Indeed, we can highlight three zones for Ni enrichment: i) a zone of plateau where Ni co-precipitated with goethite, followed at pH higher than six by ii) a peak and iii) a decrease up to the value of Ni concentration in parent rock. Of course, since we investigate a cell stand alone, it has not any income of the elements from the upper cells as it was in a column modelling, but the principal shape of Ni enrichment curve will remain the same with some differences in values. This shape, shown in Figure 7(*A*), is very close to that presented in Figure 1. Similarly as it is observed in the field, the zone of residual laterites (Fig.7(*A*)) is mostly composed of iron

oxy-hydroxides, and Ni, being more mobile, reaches its maximum concentrations at the base of this region. This area is marked by a sharp increase in pH and subsequently MgO content (Fig.7(*A*)). The latter means that pH appears to be the most important chemical parameter that drives the enrichment of nickel in the weathering profile. Nevertheless, some differences can be spotted in between Figure 7(*A*) and Figure 1 chemical distributions. First and foremost, as one can see, oxide Ni deposits show a regular decrease of bulk nickel content towards the surface (Fig.1) (*e.g.* Trescases (1973); Wells et al. (2009); Dublet et al. (2012)), while Figure 7(*A*) with the modelling results represents a stable plateau with value of 2 wt.% of Ni. Dublet et al. (2012) have explained it by ageing of goethite in situ through successive dissolution and precipitation cycles during lateritization. Due to a strong mismatch with Fe^{3+} both in terms of ionic radii and valence, nickel, substituted for Fe in goethite, is likely to be expelled during each dissolution/precipitation cycle which leads to purification and increase of crystallinity of goethite. In addition, such a decrease in Ni content might be related to the fact that some part of Ni in nature is also bonded in Mn-oxides (up to 10 %). As far as these Mn-oxides are more soluble than iron oxy-hydroxides, they have been leached from upper limonite zone and, therefore, a consequent drop in Ni grade appears.

Another difference lies in a form of a peak and distribution of Ni concentrations around it. Here, there is a number of possible processes that might have influenced the peak shape making it smoother and wider, namely: diffusion, dispersion, convective flows, kinetics of precipitation of silicates, etc. It is important to note that the shape of nickel enrichment curve represents itself a superposition of different processes of Ni retention that are all evolving in time due to chemical conditions change. In our simulations three different concurrent fates of Ni deposition in a profile were taken into account: i) Ni in a goethite crystal lattice, ii) Ni sorbed on weak and strong goethite sorption sites, and iii) Ni precipitated with silicates (garnierite). Therefore, the superposition that represents the Ni enrichment curve (red line) in Figure 7(*A*) stands for the sum of these three processes. The contribution of each process in the total Ni enrichment is shown in Figure 7(*B*).

One can see that nickel mineralization begins with the formation of Ni-silicates at high pH, at the moment when ultramafic bedrock just starts to dissolve. At the same time the precipitation of Ni-goethite occurs, with subsequent adsorption of Ni on its surface. Due to the leaching of the elements out of the cell in course of olivine dissolution and refilling it by slightly acidic meteoric water at each time step, the pH in a modelled cell tends to decrease. Thus, according to the Figure 7(*B*), at pH value above 9, Ni retention triggered by silicates precipitation prevails over the other processes. Then, the retention of nickel in goethite lattice becomes increasingly important with the maximum achieved at pH 6 and lower. In between these two important mechanisms, there is another one, related to adsorption of Ni on goethite. This process has its specific place during the weathering (Fig.7(*B*)); it appears where pH is high enough to have sufficient charge of oxide surface to enhance sorption for binding of nickel. At the same time, at the values of pH of 8.5 or higher, it seems to be inhibited by some other process and subsequently replaced by precipitation of Ni-silicate (Fig.7(*B*)). Therefore, adsorption is being rather a "transitional ore" since being released from silicates the adsorbed nickel further passes to the lattice of goethite or precipitates with it. As it has been noticed previously, the pH front in the nature most likely represents smoother curve due to diffusion, dispersion, convective flows etc., and the window of existence of such a "transitional ore" on the surface of oxides might be geometrically larger. The following subchapter is fully devoted to understanding of adsorption process of nickel alone in batch calculations, as well as in competitive environment of transport modelling.

3.2.3. Competition of elements for sorption sites

According to the results of the 1-D numerical transport modelling, presented in chapter (3.1), adsorption of nickel strongly depends on pH (Fig.5 and 7(*B*)) and does not appear in limonite zone due to full dissolution of silicates and decrease of pH to the value of rainwater (*i.e.* 5.6). Indeed, the surfaces of oxides carry a charge that enhances sorption of metals and depends on pH and composition of the solution. Figure 8 represents a batch calculation of nickel distribution among the aqueous phase and strong/weak sorption sites of 0.09 g of goethite, while Figure 9 shows the shape of the sorption edge of Ni^{2+} as a function of pH. These calculations are based on the Gouy-Chapman model from Dzombak and Morel (1990) and show the results of distribution for low (10^{-8} M) and high (10^{-4} M) nickel concentrations. Concentrations of Ni, representative in our modelling, generally lie in this interval, being lower than 10^{-6} M.

As one can see from both Figures 8 and 9, nickel is more strongly sorbed at high pH values than at low pH values. The shape of the sorption edge is shown in Figure 9 and actually depends on the Ni concentration. At low concentrations (e.g. 10^{-8} M) the pH domain where Ni is sorbed to the surface of goethite increases from

pH 8 to 10.5 while at higher concentrations it reduces, general shape of the Ni sorption edge smooths, and the acid branch shifts to the higher pH.

This is related to the fact that adsorption of high Ni concentrations also occurs on weak sites, what can be seen from the Figure 8. Indeed, the distribution of Ni among the solution and sorption sites of goethite does also depend on the Ni concentration. At low concentrations of nickel (Fig.8(*A*)) the strong binding sites outcompete the weak binding sites over the entire pH range. Therefore, at high pH, most of the nickel resides at the strong binding sites. In case of larger nickel concentrations (Fig.8(*B*)), the strong binding sites prevail only at low pH.

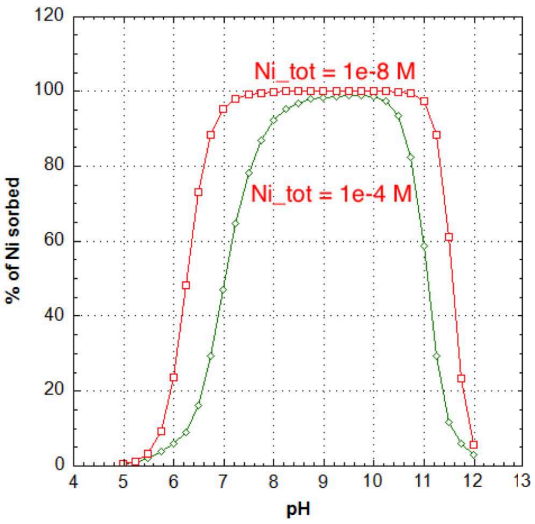

Figure 9: The sorption edge of (10^{-8} M) and (10^{-4} M) Ni^{2+} at the surface of 0.09 g of goethite (ferrihydrite) as a function of pH in 0.1M NaCl solution.

Surface complexation theory appears to be a useful tool, helping to obtain a conceptual understanding of metal sorption behavior on mineral surfaces. While previous model (Fig.8 and 9) was oversimplified representing closed system, fixed goethite amount, and showing a sorption just for Ni, assumed to be the only metal in solution, the following one deals with competition of metals for sorption sites in a real case. The phenomenon is highlighted in Figure 10, where reactive transport modelling has been performed through one cell with flux-open boundaries as in previous subchapter (3.2.2).

With the subsequent decrease of pH magnesium releases again into pore water, giving way to Ni adsorption, which has a maximum at pH of 8.5. It appears that at higher values of pH the Ni adsorption is inhibited by Mg binding, which competes with Ni for the sorption sites. At lower ones nickel is released to pore water due to the decrease of surface charge. In this way at pH equal 6 all Ni has left goethite sorption sites, which explains why no Ni sorption occur in the 1-D column (Fig. 5 and 7) before pH front (pH 5.6).

Once the goethite has been formed in the system, adsorption starts to regulate the mobility of metals and retarding their movement. As can be seen in Figure 10, Mg at some point starts occupying weak sites of goethite, attaining maximum at pH of about 9.2 where, as it was shown in Figure 9, nickel, being alone in the system, would have attained its maximum sorption.

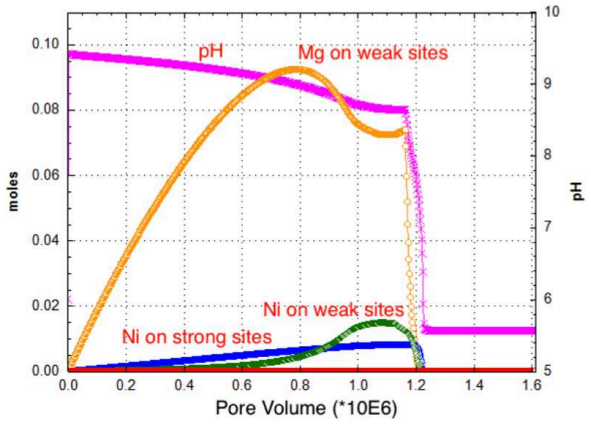

Figure 10: Competition of Mg and Ni for sorption sites of goethite, based on the 1-D transport through 1 cell as in a subchapter 3.2.2.

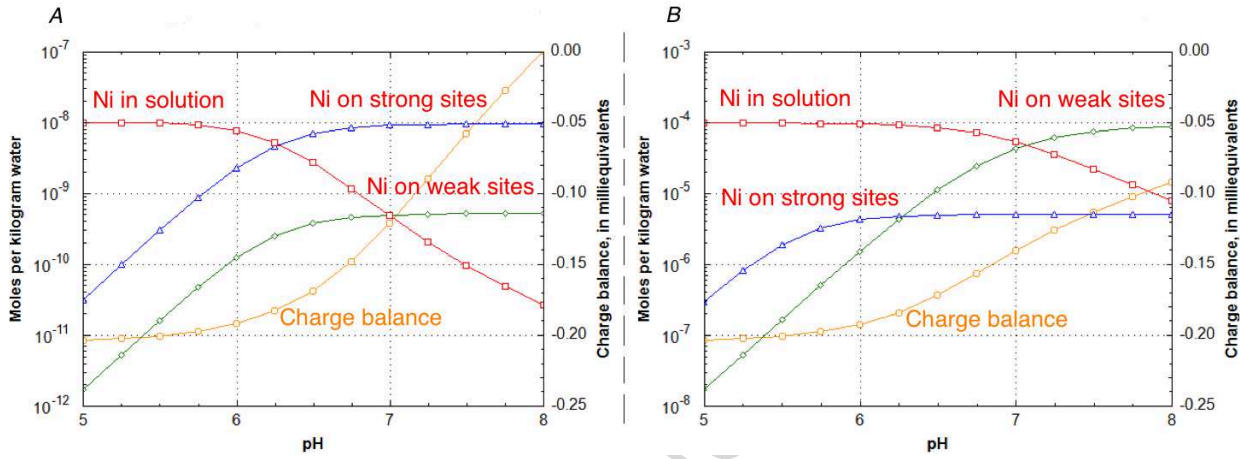

Figure 8: Distribution of Ni among the aqueous phase and strong/weak surface sites of goethite (ferrihydrite) as a function of pH. Picture on the left (***A***) corresponds to low Ni concentration (10^{-8} M), while ***B*** represents high Ni concentration (10^{-4} M). Additional Y-axis represents charge balance of the solution. Solution was prepared with 0.1M NaCl, which permits to use HCl or NaOH as reactant to keep pH increasing, and 90 mg pre-equilibrated ferrihydrite.

Thus, to conclude, adsorption of nickel on oxy-hydroxide surfaces (goethite) should not be regarded for Ni alone due to the big influence of other cations releasing during the ultramafic bedrock alteration, in particular Mg. This competition of cations for the sorption sites is to large extent controlled by pH. Adsorption of Ni becomes important in a restricted range of pH around 8, quickly releasing at lower than neutral pH values to pore water and being minor due to competition with Mg at higher ones.

4. Conclusions

The formation of Ni laterite profile from ultramafic parent rock, at 25°C, has been simulated by means of Phreeqc one-dimensional reaction-transport code. The main conclusions are listed below:

- The downward progression of the pH front controls thickening of iron-rich zone, explains the mobility of the elements and governs the Ni enrichment.
- Precipitation of talc-like silicates at the expense of sepiolite-like at 25°C is favored by high pH due to dissolution of still persisting olivine.
- The use of separate silicate phases instead of their solid solutions in the simulations may be considered as reliable since it does not have a drastic effect on the global Ni mass balance.
- Modeling of Ni co-precipitation with goethite explains the presence of Ni in upper limonite zone, where adsorption cannot retain Ni anymore due to acidic pH. The decrease of bulk NiO content towards the surface might be explained by ageing of goethite in situ through successive dissolution and precipitation cycles during lateritization and also by dissolution of Mn oxides.
- Adsorption is being rather a “transitional ore” since after its release from silicates the adsorbed nickel further passes to the lattice of goethite or precipitates with it. The process is fully controlled by pH front and its shape.
- Nickel is more strongly adsorbed at high pH values than at low pH values up to some limit, when alone in the system.
- Adsorption of Ni becomes significant in a narrow range of pH due to the competition of Mg and Ni for sorption sites of goethite surface. Thus, it is of importance to take into account the competition between cations for sorption sites during the ultramafic bedrock alteration

Presented in this paper reactive transport modelling of secondary nickel ore development is rather homogeneous (constant temperature, 1D flow) and aims at understanding the main chemical and hydrological influence on it. Further successive dissolution and precipitation cycles of the minerals during lateritization are very closely tied to inherited ores, tectonics, formation

of preferential pathways, lateral movement, change of relief, higher temperatures, that might explain ore distribution heterogeneities observed on many Ni-laterite sites. Therefore, 2D/3D reactive transport simulations will be conducted to assess these aspects based on a coupling approach between geochemistry, hydrodynamics and heat and mass transfer.

Acknowledgments

This work has been supported by the French National Research Agency through the national program "Investissements d'avenir" with the reference ANR-10-LABX-21-01 / LABEX RESSOURCES21.

References

Barrow, N. J., Gerth, J., and Brümmer, G. W. (1989). Reaction kinetics of the adsorption and desorption of nickel, zinc and cadmium by goethite. 2. Modeling the extent and rate of reaction. *J. Soil Sci.*, 40:437–450.

Brantley, S. L. and Chen, Y. (1995). Chemical weathering rates of pyroxenes and amphiboles. *Reviews in Mineralogy*, 31:119–172.

Brümmer, G. W., Gerth, J., and Tiller, K. G. (1988). Reaction kinetics of the adsorption and desorption of nickel, zinc and cadmium by goethite. I. Adsorption and diffusion of metals. *J. Soil Sci.*, 39:37–51.

Butt, C. R. M. and Cluzel, D. (2013). Nickel laterite ore deposits: Weathered serpentinites. *Elements*, 9:123–128. http://dx.doi.org/10.2113/gselements.9.2.123.

Carvalho-e-Silva, M. L. M., Ramos, A. Y., Nogueira Tolentino, H. C., Enzweiler, J., Netto, S. M., and Martins Alves, M. C. (2003). Incorporation of Ni into natural goethite: An investigation by X-ray absorption spectroscopy. *Am Mineral*, 88:876–882. DOI: 10.2138/am–2003–5–617.

Cathelineau, M., Caumon, M. C., Massei, F., Brie, D., and Harlaux, M. (2015). Raman spectra of Ni-Mg kerolite: effect of Ni-Mg substitution on O-H stretching vibrations. *J. Raman Spectrosc*, 46 (10):933–940.

Cathelineau, M., Quesnel, B., Gautier, P., Boulvais, P., Couteau, C., and Drouillet, M. (2016). Nickel dispersion and enrichment at the bottom of the regolith: formation of pimelite target-like ores in rock block joints (Koniambo Ni deposit, New Caledonia). *Mineralium Deposita*, 51 (2):271–282.

Cornell, R. M. (1991). Simultaneous incorporation of Mn, Ni and Co in the goethite (α - FeOOH) structure. *Clay Miner*, 26:427–430.

Cornell, R. M., Giovanoli, R., and Schneider, W. (1992). The effect of nickel on the conversion of amorphous iron(iii) hydroxide into more crystalline iron oxides in alkaline media. *Journal of Chemical Technology and Biotechnology*, 53:73–79.

Davis, J. A., Fuller, C. C., and Cook, A. D. (1987). A model for trace metal sorption processes at the calcite surface: Adsorption of Cd and subsequent solid solution formation. *Geochim. Cosmochim. Acta*, 51:1477–1490.

Domènech, C., Galí, S., Villanova-de Benavent, C., Soler, J. M., and Proenza, J. A. (2017). Reactive transport model of the formation of oxide-type nilaterite profiles (punta gorda, moa bay, cuba). *Mineralium Deposita*, pages 1–18.

Dublet, G., Juillot, F., Morin, G., Fritsch, E., Fandeur, D., and Brown, J. G. (2015). Goethite aging explains Ni depletion in upper units of ultramafic lateritic ores from New Caledonia. *Geochim Cosmochim Ac*, 160:1–15.

Dublet, G., Juillot, F., Morin, G., Fritsch, E., Fandeur, D., Ona-Nguema, G., and Brown, J. G. (2012). Ni speciation in a New Caledonian lateritic regolith: A quantitative X-ray absorption spectroscopy investigation. *Geochim Cosmochim Ac*, 95:119–133.

Dzombak, D. A. and Morel, F. M. M. (1990). *Surface Complexation Modeling:Hydrous Ferric Oxide*. New York, John Wiley and Sons.

Fischer, L., Brümmer, G. W., and J, B. N. (2007). Observations and modelling of the reactions of 10 metals with goethite: adsorption and diffusion processes. *Eur J Soil Sci*, 58:1304–1315. doi: 10.1111/j.1365– 2389.2007.00924.x.

Fletcher, R. C., Buss, H. L., and Brantley, S. L. (2006). A spheroidal weathering model coupling porewater chemistry to soil thicknesses during steady-state denudation. *Earth Planet Sci Lett*, 244:444–457.

Freyssinet, P., Butt, C. R. M., Morris, R. C., and Piantone, P. (2005). Ore-forming processes related to lateritic weathering. *Economic Geology*, 100th Anniversary Volume:681–722.

Galí, S., Soler, J. M., Proenza, J. A., Lewis, J. F., Cama, J., and Tauler, E. (2012). Ni-enrichment and stability of Al-free garnierite solid solutions: a thermodynamic approach. *Clays Clay Miner*, 60:121–135.

Gerth, J., Brümmer, G. W., and Tiller, K. G. (1993). Retention of Ni, Zn and Cd by Si-associated goethite. *Z. Pflanzenern. Bodenk.*, 156:123–129.

Gleeson, S. A., Butt, C., and Elias, M. (2003). Nickel laterites: A review. *SEG Newsletter*, 54:9–16.

Glynn, P. D. (2000). Solid-solution solubilitites and thermodynamics: sulfates, carbonates and halides. *Rev.Mineral.*, 40:481–511.

Golightly, J. P. (1981). Nickeliferous laterite deposits. *Economic Geology*, 75th anniversary volume:710–735.

Golightly, J. P. (2010). Progress in understading the evolution of nickel laterites. *Society of Economic Geologists Special Publication*, 15:451–485.

Golubev, S. V., Pokrovsky, O. S., and Schott, J. (2005). Experimental determination of the effect of dissolved CO_2 on the dissolution kinetics of Mg and Ca silicates at 25 °C. *Chem. Geol*, 217:227–238.

Guilbert, J. M. and Park, C. F. (1986). *The geology of ore deposits. 4th ed.* New York : W.H. Freeman.

Herzberg, C., Asimow, P. D., Ionov, D. A., Vidito, C., Jackson, M. G., and Geist, D. (2013). Nickel and helium evidence for melt above the core-mantle boundary. *Nature*, 493:393–397.

Jeanpert, J. and Dewandel, B. (2013). Analyse préliminaire des donées hydrogéologiques du massif du Koniambo. *Public Report BRGM/RP-61765-FR*, page 102p.

Johnson, J., Anderson, G., and Parkhurst, D. (2000). Database from thermo.com.v8.r6.230 prepared at lawrence livermore national laboratory. (Revision: 1.11).

Join, J.-L., Robineau, B., Ambrosi, J.-P., Costis, C., and Colin, F. (2005). Système hydrogéologique d'un massif minier ultrabasique de nouvelle-calédonie. *Comptes Rendus Geoscience*, 337(16):1500–1508.

Jones, B. F. (1986). Clay mineral diagenesis in lacustrine sediments. *Studies in Diagenesis. U.S. Geol. Surv. Bull.*, 1578:291–300.

Lebedeva, M. I., Fletcher, R. C., Balashov, V. N., and L, B. S. (2007). A reactive diffusion model describing transformation of bedrock to saprolite. *Chem Geol*, 244:624–645.

Lelong, F., Tardy, Y., Grandin, G., Trescases, J. J., and Boulange, B. (1976). Pedogenesis, chemical weathering and processes of formation of some supergene ore deposits, in Wolf K.H., ed., supergene and surficial ore deposits.Texture and fabrics. *Handbook of strata-bound and stratiform ore deposits: Amsterdam, Elsevier*, v. 3:93–133.

McKenzie, R. (1980). The adsorption of lead and other heavy metals on oxides of Mn and Fe. *Aust. J. Soil Res.*, 18:61–73.

Navarre-Sitchler, A., Steefel, C. I., Sak, P. B., and Brantley, S. L. (2011). A reactive-transport model for weathering rind formation on basalt. *Geochim Cosmochim Ac*, 75:7644–7667 doi:10.1016/j.gca.2011.09.033.

Nriagu, J. O. (1975). Thermochemical approximation for clay minerals. *American Mineralogist*, 60:834–839.

Parkhurst, D. L. and Appelo, C. A. J. (2013). Description of input and examples for PHREEQC version 3-A computer program for speciation, batch-reaction, one-dimensional transport, and inverse geochemical calculations. *U.S. Geological Survey Techniques and Methods*, book 6, chap. A43, 497 p., available only at http://pubs.usgs.gov/tm/06/a43/.

Pokrovsky, O. S. and Schott, J. (2000). Kinetics and mechanism of forsterite dissolution at 25°C and pH from 1 to 12. *Geochim. Cosmochim. Acta*, 64:3313–3325.

Quesnel, B., Boulvais, P., Gautier, P., Cathelineau, M., Cdric, M. J., Dierick, M., Agrinier, P., and Drouillet, M. (2015). Formation of silica and magnesite veins in the Massif of Peridotite of Koniambo: Geometric and stable isotopes data. *13th SGA Biennial Meeting 2015. Proceedings*, 3:1189–1192.

Reddy, B. J., Frost, R. L., and Dickfos, M. J. (2009). Characterisation of Ni silicate-bearing minerals by UV- vis-NIR spectroscopy. Effect of Ni substitution in hydrous Ni-Mg silicates. *Spectrochimica Acta Part A: Molecular and Biomolecular Spectroscopy*, 71(5):1762–1768.

Schultz, M. F., Benjamin, M. M., and Ferguson, J. F. (1987). Adsorption and desorption of metals on ferrihydrite: Reversibility of reaction and sorption properties of the regenerated solid. *Env. Sci. Technol*, pages 663–669.

Schwertmann, U. and Murad, E. (1983). Effect of pH on the formation of goethite and hematite from ferrihydrite. *Clays and Clay Minerals*, 31(4):277–284.

Singh, B., Sherman, D. M., and Gilkes, R. J. (2002). Incorporation of Cr, Mn and Ni into goethite (α -FeOOH): Mechanism from extended X-ray absorption fine structure spectroscopy. *Clay Miner.*, 37:639–649.

Soler, J. M. and Lasaga, A. C. (1996). A mass transfer model of bauxite formation. *Geochim Cosmochimi Ac*, 60:4913–4931.

Soler, J. M. and Lasaga, A. C. (1998). An advection-dispersion-reaction model of bauxite formation. *J Hydrol*, 209:311–330.

Springer, G. (1974). Compositional and structural variations in garnierites. *The Canadian Mineralogist*, 12:381–388.

Springer, G. (1976). Falcondoite, nickel analogue of sepiolite. *The Canadian Mineralogist*, 14:407–409.

Stipp, S. L. S., Hochella, M. F., Parks, G. A., and Leckie, J. O. (1992). Cd uptake by calcite, solid-state diffusion, and the formation of solid-solution: Interface processes observed with near-surface sensitive techniques (XPS, LEED and AES). *Geochim. Cosmochim. Acta*, 56:1941–1954.

Stoessell, R. K. (1988). 25°C and 1 atm dissolution experiments of sepiolite and kerolite. *Geochimica et Cosmochimica Acta*, 52:365–374.

Swamy, Y., Kar, B. B., and Mohanty, J. K. (2003). Physico-chemical characterization and sulphatization roasting of low-grade nickeliferous laterites. *Hydrometallurgy*, 69:89–98.

Thom, J. G. M., Dipple, G. M., Power, I. M., and Harrison, A. L. (2013). Chrysotile dissolution rates: Implications for carbon sequestration. *Applied Geochemistry*, 35:244–254.

Thorne, R. L., Roberts, S., and Herrington, R. (2012). Climate change and the formation of nickel laterite deposits. *Geology*, 40:331–334.

Trescases, J. J. (1973). Weathering and geochemical behaviour of the elements of ultramafic rocks in New Caledonia. *Bureau Mineral Res Geol Geophys Dep Mineral Energy Canberra Bull*, 141:149–161.

Trescases, J. J. (1975). *L'élvolution gélochimique supergèlne des roches ultrabasiques en zone tropicale: Formation des gisements nickélifères de Nouvelle-Calédonie: Mémoires ORSTOM (Office de la Recherche Scientifique et Technique Outre-Mer)*. PhD thesis.

Troly, G., Esterle, M., Pelletier, B., and Reibel, W. (1979). Nickel deposits in New Caledonia: some factors influencing their formation. *International Laterite Symposium, New Orleans,*, pages 85–119.

Ulrich, M. (2010). *Péridotites et serpentinites du complexe ophiolitique de la Nouvelle-Calédonie*. PhD thesis, Université de la Nouvelle-Calédonie et Université de Grenoble.

Ulrich, M., Muñoz, M., Guillot, S., Chauvel, C., Cluzel, D., and Picard, C. (2011). Weathering effects on the mineralogical and geochemical composition of the New Caledonia ophiolite. *Goldschmidt Conference*.

Villanova-de-Benavent, C., Proenza, J. A., Galí, S., Garca-Casco, A., Tauler, E., Lewis, J. F., and Longo, F. (2014). Garnierites and garnierites: Textures, mineralogy and geochemistry of garnierites in the Falcondo Ni-laterite deposit, Dominican Republic. *Ore Geology Reviews*, 58:91–109.

Wells, M. A., Ramanaidou, E. R., Verrall, M., and Tessarolo, C. (2009). Mineralogy and crystal chemistry of garnierites in the Goro lateritic nickel deposit, New Caledonia. *Eur. J. Mineral.*, 21:467–483.

Wilson, M. (2004). Weathering of the primary rock-forming minerals: Processes, products and rates. *Clay Minerals*, 39:233–266.

Wogelius, R. A. and Walther, J. V. (1991). Olivine dissolution at 25°C - effects of pH, CO_2, and organic-acids. *Geochim. Cosmochim. Acta*, 55:943–954.

Highlights

- Development of 1D reactive transport model for studying Ni mineralization processes in the laterite profiles.
- Assessment of Ni distribution in between different fluid-rock interactions processes. Key chemical parameters that control the formation.
- The comparative role of adsorption and incorporation of Ni in goethite upon the formation of laterite.